Nano Research 2015, 8(8): 2503–2514
DOI 10.1007/s12274-015-0758-2
Research Article
ISSN 1998-0124
CN 11-5974/O4

Monodisperse core-shell structured magnetic mesoporous aluminosilicate nanospheres with large dendritic mesochannels

Jianping Yang[1,2,3], Dengke Shen[2,4], Yong Wei[2], Wei Li[2], Fan Zhang[2], Biao Kong[2], Shaohua Zhang[3], Wei Teng[1], Jianwei Fan[1], Weixian Zhang[1] (✉), Shixue Dou[3], and Dongyuan Zhao[2] (✉)

[1] *College of Environmental Science and Engineering, State Key Laboratory of Pollution Control and Resources Reuse, Tongji University, Shanghai 200092, China*
[2] *Department of Chemistry, Shanghai Key Laboratory of Molecular Catalysis and Laboratory of Advanced Materials, Fudan University, Shanghai 200433, China*
[3] *Institute for Superconducting & Electronic Materials, Australian Institute of Innovative Materials, University of Wollongong, Innovation Campus, Squires Way, North Wollongong, NSW 2500, Australia*
[4] *Key Laboratory of Materials Physics, Centre for Environmental and Energy Nanomaterials, Anhui Key Laboratory of Nanomaterials and Nanotechnology, Institute of Solid State Physics, Hefei Institutes of Physical Science, Chinese Academy of Sciences, Hefei 230031, China*

Received: 22 January 2015
Revised: 17 February 2015
Accepted: 1 March 2015

KEYWORDS
mesoporous materials, core-shell structures, aluminosilicates, magnetic property, surface acid

ABSTRACT

The rational design and precise synthesis of multifunctional hybrid nanostructures with a tailored active core and a large, dendritic, modified mesoporous structured shell can promote catalysis, energy storage, and biological applications. Here, an oil-water biphase stratification coating strategy has been developed to prepare monodisperse magnetic dendritic mesoporous silica core-shell structured nanospheres. These sophisticated Fe_3O_4@SiO_2@dendritic-mSiO_2 nanospheres feature large dendritic open pores (2.7 and 10.3 nm). Significantly, the silica shells can be converted into dendritic mesoporous aluminosilicate frameworks with unchanged porosity, a Si/Al molar ratio of 14, and remarkably strong acidic sites, through a post-synthesis approach. In addition, the resultant magnetic dendritic mesoporous aluminosilicate nanospheres exhibit outstanding properties and promising application in phosphate removal from wastewater.

1 Introduction

Core-shell structures with a functionalized interior core and permeable outer shell have recently emerged as ideal and powerful platforms for various applications [1], such as nanoreactors [2], confined catalysis [3], controlled release and energy storage [4], owing to their unique and fascinating properties of spatially

Address correspondence to Weixian Zhang, zhangwx@tongji.edu.cn; Dongyuan Zhao, dyzhao@fudan.edu.cn

designable distribution, multi-functionality, high surface area, and permeability [5]. The success of these widespread applications is highly dependent on the availability and permeability of multifarious shell architectures with a desirable structure [6], composition, and thickness, which are integrated with well-designed functional cores [7–9]. Up to now, a variety of shell architectures, for materials including noble metals [10], semiconductors [11], polymers [12–17], carbon [18], and silica [19, 20], and general strategies have been developed to prepare core-shell structures with diverse morphologies, tailored compositions, and outstanding applications [21–26]. Among these, mesoporous silica shells with high surface area, large pore volume, adjustable pore size, superior surface properties, and biocompatibility have received increasing attention in recent years [27]. Notably, these mesoporous silica core-shell structures with open and accessible mesopore channels not only facilitate the loading of additional guest materials and promote the penetration of mass diffusion and reactant transport, but also make the active surface of the functional core directly accessible to realize synergistic effects [28–31].

Currently, many synthesis approaches have been successfully developed to fabricate mesoporous silica-coated core-shell structures [32]; for example, partial etching of silica shells to create random mesopores [33], and calcination with a mesostructure-directing agent, n-octadecyltrimethoxysilane (C_{18}TMS), to form disordered pore channels [34] have been investigated. One general strategy for ordered mesoporous silica shells is a surfactant-templating route. For example, the cationic surfactant hexadecyltrimethylammonium bromide (CTAB) is commonly adopted through a templating-Stöber sol-gel process to realize mesoporous silica coatings with highly open and ordered mesopores [35–38]. However, the small pore size (around 2 nm) due to the limited length of the alkyl chains of the CTAB surfactant, greatly restricts the use of these coating in applications that involve macromolecules [39]. The ideal surfactants are nonionic triblock copolymers, which offer larger mesopores (>7 nm) via a templating-assembly approach [40]. Unfortunately, these assembly processes tend to promote aggregation and need to be conducted in a harsh acidic medium (HCl or boric acid) [40–42], which makes them sensitive to the choice of functional cores, and thereby, hinders the extension of these routes. Therefore, it remains a great, but worthwhile, challenge the development of effective synthesis strategies for preparing monodisperse mesoporous silica core-shell structures with large and open mesopore channels [9].

Moreover, it is rare for the work to succeed in a sufficient utilization and rational design of the alterable mesopore shells [43]. In fact, mesoporous silicas present abundant hydroxyl groups, accompanied by well-controlled hydrolysis and condensation chemistry, and excellent surface properties. These remarkable features provide opportunities to develop various methods for the modification of the mesoporous silica shell with new structures, properties, and extended applications. Furthermore, to realize the synergistic effects, the rational design and fabrication of core-shell structures with a functionalized interior core and chemically modified mesoporous shell have been continuously pursued. In addition, dendritic silica with gradually increasing pore size from the core to the surface provides center-radial large pore channels, and hierarchical and highly accessible pore structures [44]. The combination of such unique properties with functional components to form core-shell architectures is highly desirable for significant multifunctional platforms [44–48].

Very recently, dendritic-like large-pore mesoporous silica, and organosilica nanospheres have successfully been prepared through an oil-water biphase stratification approach. Such facile biphase synthesis system not only enables the cooperative self-assembly between surfactant and precursors, which occurs at the interface, but also allows the upper hydrophobic oil phase to act as the swelling agents to create large mesopores [44, 45, 48, 49]. Herein, we report an effective method for the synthesis of monodisperse magnetic dendritic mesoporous silica core-shell structured nanospheres (denoted as Fe_3O_4@SiO_2@dendritic-mSiO_2) through an oil-water biphase stratification coating strategy, as shown in Scheme 1. Such unique core-shell structures exhibit notable features: i) the preservation of the core with a strong magnetic response (~15.2 emu·g^{-1}); ii) the presence on the shell of dendritic, hierarchical, radially oriented, and large mesopores (2.7 and 10.3 nm); iii) well-dispersibility, high surface area (395.8 m^2·g^{-1}),

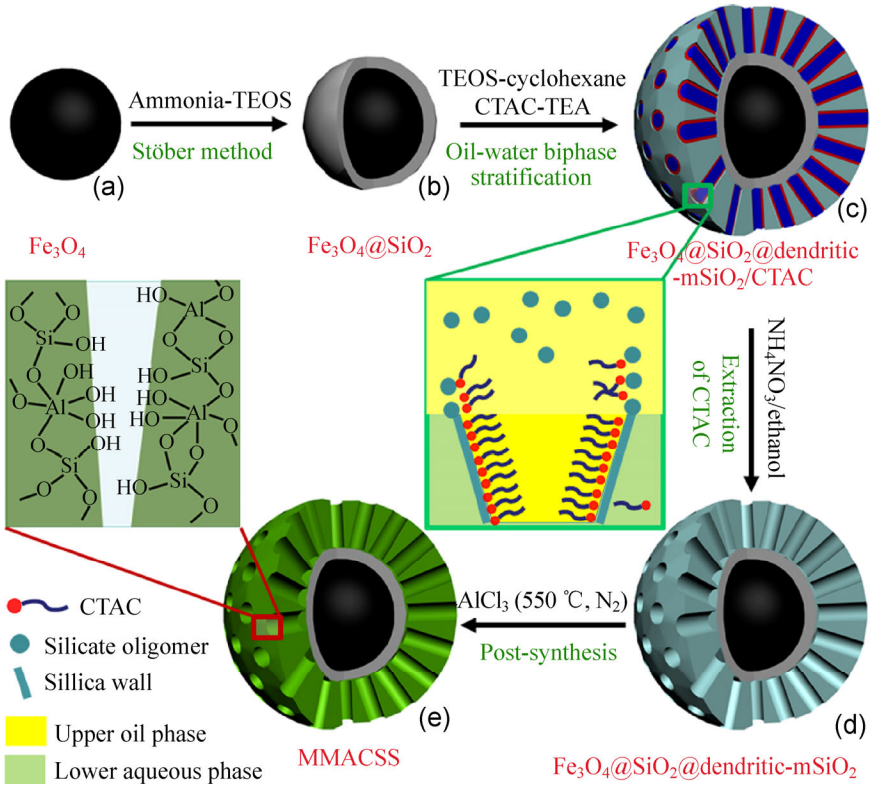

Scheme 1 Synthetic procedure for the monodisperse MMACSS nanospheres by combining oil-water biphase stratification with a post-synthesis strategy.

and large pore volume (0.54 $cm^3 \cdot g^{-1}$); iv) easy modification of the fascinating dendritic silica channels. In a further case, the large and dendritic mesoporous silica layer can be converted into an aluminosilicate shell via a post-synthesis approach with unchanged porosity. Furthermore, owing to the integration of Al into the mesostructure frameworks, the monodisperse magnetic mesoporous aluminosilicate core-shell structured (MMACSS) nanospheres present excellent phosphate removal capacity (12.7 $mg \cdot g^{-1}$) and rapid kinetic equilibrium (50 min).

2 Experimental

2.1 Materials

All the chemicals were of analytical grade and used without further purification. $FeCl_3$, trisodium citrate, sodium acetate, ethylene glycol, 2-propanol, cyclohexane, and $Al(Cl)_3 \cdot 6H_2O$ were obtained from Sinopharm Chemical Reagent Co., Ltd. Tetraethyl orthosilicate (TEOS), ammonia aqueous solution (28 wt.%), cetyltrimethylammonium chloride (CTAC) solution (25 wt.% in H_2O), and triethanolamine (TEA) were purchased from Sigma-Aldrich (UK). Deionized water was used in all the experiments.

2.2 Methods

2.2.1 *Preparation of Fe_3O_4 nanoparticles*

Highly water-dispersible magnetite nanospheres with a diameter of approximately 160 nm were prepared through a solvothermal method using $FeCl_3$ as the iron source and trisodium citrate as a stabilizer in ethylene glycol solution. Typically, 3.25 g of $FeCl_3$ and 1.2 g of trisodium citrate were dissolved in 100 mL of ethylene glycol. Subsequently, 6 g of sodium acetate was added and vigorously stirred for 1 h to form a clear solution. Afterwards, the solution was distributed into four 30-mL Teflon-sealed autoclaves, and solvothermally treated at 200 ℃ for 10 h in an oven. The black products were obtained after the autoclaves were cooled to room temperature, and sequentially washed with ethanol and water for three cycles.

2.2.2 Synthesis of Fe_3O_4@SiO_2 core-shell nanospheres

In a typical synthesis of the middle layer, namely, a silica coating with a thickness of approximately 20 nm, 0.15 g of Fe_3O_4 nanospheres was added to 200 mL of 2-propanol solution and treated ultrasonically for 30 min. The dispersed solution was then transferred to an oil bath at 40 ℃ and mechanically stirred at a speed of 600 rpm. Subsequently, 10 mL of ammonia aqueous solution (28 wt.%) and 18 mL of H_2O were dropped into the dispersion. After stirring for 30 min, 0.5 mL of TEOS was rapidly injected, and the reaction continued for 2 h. The Fe_3O_4@SiO_2 nanospheres were magnetically separated, and finally obtained after washing with ethanol and water for three times.

2.2.3 Synthesis of Fe_3O_4@SiO_2@dendritic-mSiO_2 core-shell nanospheres

The dendritic silica shells with large mesopores were coated on the surfaces of the Fe_3O_4@SiO_2 nanospheres through an oil-water biphase stratification approach by using CTAC as the surfactant template in an alkaline system. In brief, 0.15 g of Fe_3O_4@SiO_2 nanospheres was added into a mixed solution containing 36 mL of H_2O, 24 mL of 25 wt.% CTAC/H_2O, and 0.18 mL of TEA, ultrasonicated for 0.5 h, and stirred at 60 ℃ for 1 h. Afterwards, 20 mL of TEOS (10 *v*/*v*% in cyclohexane) was gently dropped into the upper solution and capped with a condenser pipe. The system was reacted at 60 ℃ for 12 h in an oil bath with gentle mechanical stirring (200 rpm) under reflux conditions. The products were collected with magnetic separation, and then washed with ethanol and water for several cycles. The template CTAC surfactants and hydrophobic organic phase in the mesopore channels were removed through a solvent extraction method by using 6 g·L^{-1} of NH_4NO_3/ethanol solution refluxed at 60 ℃ for 10 h. This extraction process was repeated twice to obtain the Fe_3O_4@SiO_2@dendritic-mSiO_2 core-shell nanospheres.

2.2.4 Preparation of Fe_3O_4@SiO_2@dendritic-mSiO_2-Al core-shell nanospheres

The dendritic aluminosilicate shells with large mesopores were fabricated via a post-synthesis approach by using aluminum trichloride as the Al source. In a typical procedure, 0.5 g of Fe_3O_4@SiO_2@dendritic-mSiO_2 core-shell nanospheres were mixed with 0.2 g of $Al(Cl)_3 \cdot 6H_2O$ and 2.0 mL of H_2O to form a slurry. After that, the mixed slurry was ultrasonicated for 1 h and dried at 80 ℃ in air. The large mesoporous aluminosilicate shell coated Fe_3O_4@SiO_2 (MMACSS) nanospheres were obtained after a calcination treatment at 550 ℃ for 6 h under nitrogen atmosphere.

2.2.5 Adsorption of phosphate

Thermodynamic and kinetic adsorption of phosphates on the Fe_3O_4@SiO_2@dendritic-mSiO_2 and mesoporous aluminosilicate nanospheres was performed at room temperature. The adsorption isotherm experiments were conducted with 2.0 mg of adsorbents/5 mL phosphate solutions with different initial concentrations (0, 5, 10, 15, 20, 25, 30, 35, 40, 50, 60, 80, and 100 mg·L^{-1}). The solution was shaken in a rotating oscillator for 4 h at the speed of 200 rpm at room temperature. Afterwards, the solution was magnetically separated, and the suspension was analyzed by an ultraviolet-visible (UV–Vis) spectrophotometer at the wavelength of 700 nm. For the kinetic adsorption curve testing, 20 mg of MMACSS nanospheres was added into 50 mL of phosphate solution with a concentration of 50 mg·L^{-1}. The concentration of phosphate was monitored by using the UV–Vis spectrophotometer at a series of set times.

2.3 Characterizations

The morphologies and dispersibility of the samples were observed by field-emission scanning electron microscopy (FE-SEM) on a Hitachi S-4800 microscope (Japan). The core-shell structures and chemical compositions were further investigated by transmission electron microscopy (TEM, JEOL-2010) operated at an acceleration voltage of 200 kV. The samples were suspended in ethanol and dried on a holey carbon film on a Cu grid for TEM measurements. The ordering of the materials was characterized by small-angle X-ray scattering (SAXS) with a Nanostar U small-angle X-ray scattering system (Bruker, Germany) using Cu Kα radiation (λ = 1.54056 Å). The crystal structure and phase of the products were characterized using wide-angle X-ray diffraction (XRD, Bruker D8, Germany) with Ni-filtered Cu Kα radiation (40 kV, 40 mA). The porosity was measured by nitrogen sorption isotherms at 77 K with a Micromeritics Tristar 3020 analyzer

(USA). Before the measurements, the samples were degassed in vacuum at 180 ℃ for at least 6 h. The Brunauer-Emmett-Teller (BET) method was utilized to calculate the specific surface areas (S_{BET}), using adsorption data in a relative pressure (P/P_0) range from 0.04 to 0.2. The pore volume and pore size distributions were derived from the adsorption branches of the isotherms by using the Barrett-Joyner-Halenda (BJH) model. The total pore volume, V_t, was estimated from the amount adsorbed at the relative pressure P/P_0 of 0.995. Fourier transform infrared (FTIR) spectra were collected on a Nicolet Fourier spectrophotometer with a spectral width of 4,000–400 cm^{-1}, using KBr pellets of the solid samples. Magnetic characterization was conducted by superconducting quantum interference device (SQUID) magnetometry. ^{27}Al solid-state nuclear magnetic resonance (NMR) experiments on the mesoporous aluminosilicate nanospheres (without the Fe_3O_4@SiO_2 cores) were performed on a VNMRS 400 WB spectrometer (USA) with a resonance frequency of 104.18 MHz, a recycling delay of 4 s, and a reference sample of $KAl(SO_4)_2{\cdot}12H_2O$. Temperature-programmed desorption of ammonia (NH_3-TPD) was also conducted on the Micromeritics analyzer. The sample was preheated under N_2 flow at 600 ℃ for 1 h, then saturated with ammonia at 50 ℃ for 1.5 h, and subsequently desorbed at the same temperature for 3 h to remove physisorbed ammonia. Finally, the TPD operation was performed from 50 to 600 ℃ at a heating rate of 10 ℃·min^{-1}. The amount of NH_3 desorbed was monitored by a thermal-conductivity detector (TCD). The phosphate concentration was monitored with a UV–Vis (Unico SQ2802) spectrophotometer.

3 Results and discussion

The monodisperse core-shell nanospheres consist of three parts, as shown in Scheme 1: (1) the functionalized interior core, i.e., an Fe_3O_4 magnetic nanosphere; (2) a middle protective layer of dense silica; (3) an ordered mesoporous silica shell with large, hierarchical, radially oriented, dendritic mesopore channels. In a typical synthesis, the easily dispersible Fe_3O_4 magnetic nanospheres (~160 nm) were coated with a dense silica layer of about 20 nm thickness via a Stöber coating approach in a basic propanol-water solution (Fig. 1(a) and Fig. S1 in the Electronic Supplementary Material (ESM)). Here, the Fe_3O_4@SiO_2 nanospheres were selected as the core for the dendritic mesoporous silica coating owing to their distinct advantages, including the magnetic properties and the well-recognized versatility of the silica layer in coating various nanostructures and morphologies to form core-shell structures. Therefore, followed by an oil-water biphase stratification coating strategy—in which the upper oil phase is the silica source (TEOS) in a hydrophobic organic solution (cyclohexane), and the lower water phase consists of an aqueous solution of the core (Fe_3O_4@SiO_2 nanospheres), a surfactant (CTAC), and a catalyst (TEA)—dendritic mesoporous silica was further deposited on the Fe_3O_4@SiO_2 nanospheres, leading to the formation of core@shell@shell sandwich structures. As revealed by the FE-SEM images, uniform core-shell Fe_3O_4@SiO_2@dendritic-mSiO_2 nanospheres can be obtained with a mean diameter of ~400 nm (Fig. 1(b)). The rough morphology and irregular craters reveal the porosity and open mesochannels on the surface, which are further confirmed by the high-magnification FE-SEM image (Fig. 1(c)). The TEM

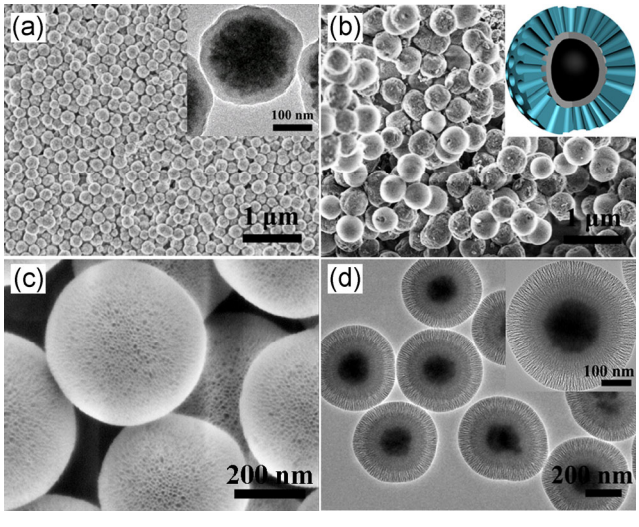

Figure 1 Scanning electron microscopy (SEM) images of (a) core-shell Fe_3O_4@SiO_2, with the TEM image in the inset, and (b) Fe_3O_4@SiO_2@dendritic-mSiO_2 nanospheres, the inset in (b) is the structural model; (c) the FE-SEM image; (d) the TEM images of the core-shell Fe_3O_4@SiO_2@dendritic-mSiO_2 nanospheres with radially oriented, large open mesochannels, and controllable pore size prepared by an oil-water biphase stratification coating strategy.

images of the core-shell Fe_3O_4@SiO_2@dendritic-mSiO_2 particles reveal highly monodisperse nanospheres with an obvious sandwich and hierarchical structure, in which a mesoporous silica shell with a thickness of ~100 nm presents dendritic radial mesopore channels with large open pores of ~10 nm in diameter (Fig. 1(d)). The SAXS pattern of Fe_3O_4@SiO_2@dendritic-mSiO_2 shows a broad scattering peak at the q-value of 0.56 nm^{-1}, indicating an ordered mesostructure (Fig. 2(a)(1)). Furthermore, this low-angle scattering peak value suggests the presence of relative large mesopores, as confirmed by the nitrogen sorption analysis. An evident and sharp capillary condensation step in the relative pressure P/P_0 range of 0.2–0.8 is observed in the nitrogen isotherms, indicating hierarchical mesopores (Fig. 2(b)(1)). The BJH model pore size distribution curve further demonstrates the hierarchical nature of the mesopore size, centered on 2.7 and 10.3 nm (Fig. 2(c)(1)). The BET surface area and total pore volume of the Fe_3O_4@SiO_2@dendritic-mSiO_2 nanospheres are calculated to be as high as 396 $m^2 \cdot g^{-1}$ and 0.54 $cm^3 \cdot g^{-1}$, respectively. Remarkably, the Fe_3O_4@SiO_2@dendritic-mSiO_2 core-shell nanospheres show superparamagnetic characteristics with a high magnetic response (~15.2 $emu \cdot g^{-1}$) (Fig. 2(d)(1)).

To provide further insight into this coating process, it can be noted that, when the TEOS content decreases from 10 to 2.5 v/v% in cyclohexane, a reduction in the thickness (from 100 to 50 nm) of the dendritic mesoporous silica shell is observed (Fig. S2(a) in the ESM). Simultaneously, the pore diameter becomes a little smaller, decreasing to 6.6 nm. These results indicate that the TEOS content plays a critical role in controlling the coating process to construct core-shell structured nanospheres with different thickness and mesopore size. Notably, the monodisperse Fe_3O_4@SiO_2@dendritic-mSiO_2 nanospheres can still be obtained with a shell thickness of ~40 nm and pore diameter of ~5.7 nm when a high concentration core (approximately in the range of 2.5–5 $mg \cdot mL^{-1}$) is added to the biphase solution (Figs. S2(b)–S2(d) in the ESM). These results reveal that the concentration of TEOS and core can also affect the shell thickness, pore size, and hierarchical structures.

To the best of our knowledge, it is difficult to fine-

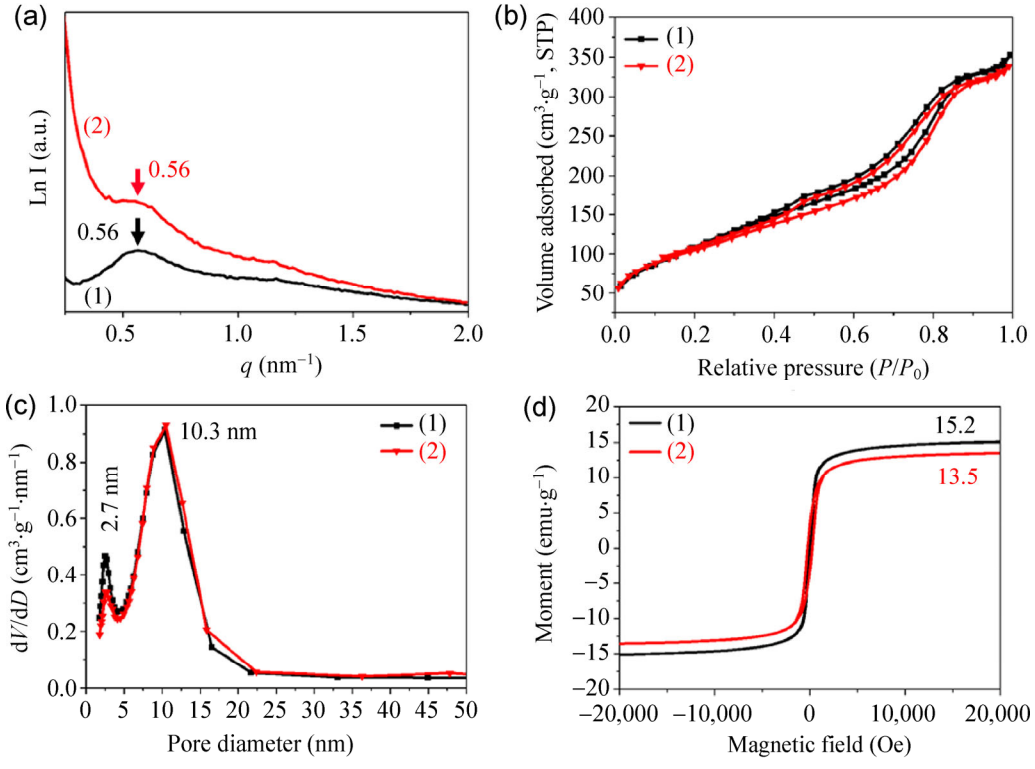

Figure 2 (a) SAXS patterns, (b) nitrogen sorption isotherms, (c) pore size distribution curves, (d) magnetic hysteresis loops of the core-shell structured Fe_3O_4@SiO_2@dendritic-mSiO_2 nanospheres (1) and magnetic mesoporous aluminosilicate core-shell structured nanospheres (2).

tune the pore diameters for mesoporous silica core-shell structures while simultaneously preserving the good dispersibility and ordered mesostructure. The oil-water biphase stratification coating strategy adopted in this work allows controlling the formation of the interfacial emulsion, slowing the hydrolysis, assembly, and growth of silicate oligomers around the surfactant/oil composites, and resulting in a uniform coating on the interface with large mesopores. For this approach, TEOS in cyclohexane oil phase can randomly diffuse from the interface to the CTAC/TEA aqueous solution and form an emulsion with continuous stirring. The contact with the TEA catalyst results in the hydrolysis of TEOS and formation of silicate oligomers at the interface of the emulsion. Then, the silicate oligomers aggregate with the CTA^+ surfactants, which are adsorbed on the surface of Fe_3O_4@SiO_2 core through electrostatic interaction. During this interfacial assembly process, the silicate oligomers continuously deposit, assemble, condense, and further grow to create the dendritic pore walls (Scheme 1(c)). In this case, the mesopore size is highly dependent on the interfacial curvature of the hydrophilic silicate oligomer/hydrophobic cyclohexane/surfactant aqueous emulsion. As a result, the pore diameters and shell thickness of these large mesopore core-shell structures can be well tailored by controlling the coating parameters, such as the TEOS content and core concentration.

In addition, the incorporation of aluminum into mesoporous silica frameworks can offer superior properties in terms of stability and acidity. Here, by a post-synthesis approach to the chemical modification of the dendritic mesoporous silica shells, the synthetic Fe_3O_4@SiO_2@dendritic-$mSiO_2$ can be utilized to fabricate MMACSS nanospheres. After calcination treatment at 550 ℃ under nitrogen atmosphere, unique monodisperse nanospheres with an unchanged size (~400 nm) are retained (Fig. S3 in the ESM). A highly-magnified FE-SEM image reveals that these well-dispersed and uniform nanospheres are full of craters on the surface, implying a highly open pore structure (Fig. 3(a)). The TEM observations clearly reveal that the aluminosilicate nanospheres possess an obvious core@shell@shell structure with a dendritic mesopore shell of ~100 nm in thickness (Fig. 3(b)). The energy-dispersive X-ray (EDX) spectra show the presence of Fe, O, Si, and Al elements, demonstrating the introduction of aluminum into the dendritic mesopore shells (Fig. 3(c)). The Si/Al molar ratio is evaluated from the EDX analysis and X-ray fluorescence to be about 14. Furthermore, the elemental mapping by EDX analysis and scanning TEM of Fe, Si, O, and Al confirms the presence of a homogeneous aluminosilicate shell on the Fe_3O_4@SiO_2 nanospheres (Figs. 3(d)–3(h)).

Notably, the incorporation of Al into the mesoporous silica shells has little effect on the mesostructure and porosity. A pronounced scattering peak is detected with an unshifted q value at 0.56 nm^{-1}, indicating that the ordered mesostructure is retained (Fig. 2(a)(2)). N_2 sorption isotherms also show the typical type-IV curves (Fig. 2(b)(2)), similar to that of the Fe_3O_4@SiO_2@dendritic-$mSiO_2$, with two narrow pore size distributions of 2.7 and 10.3 nm, (Fig. 2(c)(2)). The BET surface area and pore volume are estimated to be ~381 $m^2 \cdot g^{-1}$ and 0.53 $cm^3 \cdot g^{-1}$, respectively. The XRD pattern presents six characteristic intense diffraction peaks, which can be indexed to magnetic Fe_3O_4 with a good crystallinity (Fig. S4 in the ESM). It should be mentioned that the superparamagnetic characteristics of Fe_3O_4@SiO_2@dendritic-$mSiO_2$ change to a ferrimagnetic behavior with non-zero remanence and coercivity hysteresis for the magnetic mesoporous aluminosilicate nanospheres after the post-synthesis calcination procedure. The saturation magnetization value of the aluminosilicate nanospheres is as high as ~13.5 $emu \cdot g^{-1}$ (Fig. 2(d)(2)).

The coordination mode of Al in the aluminosilicate shells of the nanospheres was further monitored by FTIR and ^{27}Al solid-state NMR spectra. The disappearance of the absorbance bands at 2,921 and 2,850 cm^{-1}, which are indicative of the stretch vibrations of the C–H bonds of the CTAC molecules, reveals the complete removal of the surfactant templates for the Fe_3O_4@SiO_2@dendritic-$mSiO_2$ and aluminosilicate nanospheres (Fig. 4(a)(1) and 4(a)(2)). Meanwhile, for the aluminosilicate nanospheres, the silanol group at ~970 cm^{-1} disappears (Fig. 4(a)(3)), suggesting the condensation and incorporation of Al species with the silanol groups, as well as the deposition of six-coordinated Al onto the silica walls. ^{27}Al-NMR spectra of the mesoporous aluminosilicate nanospheres

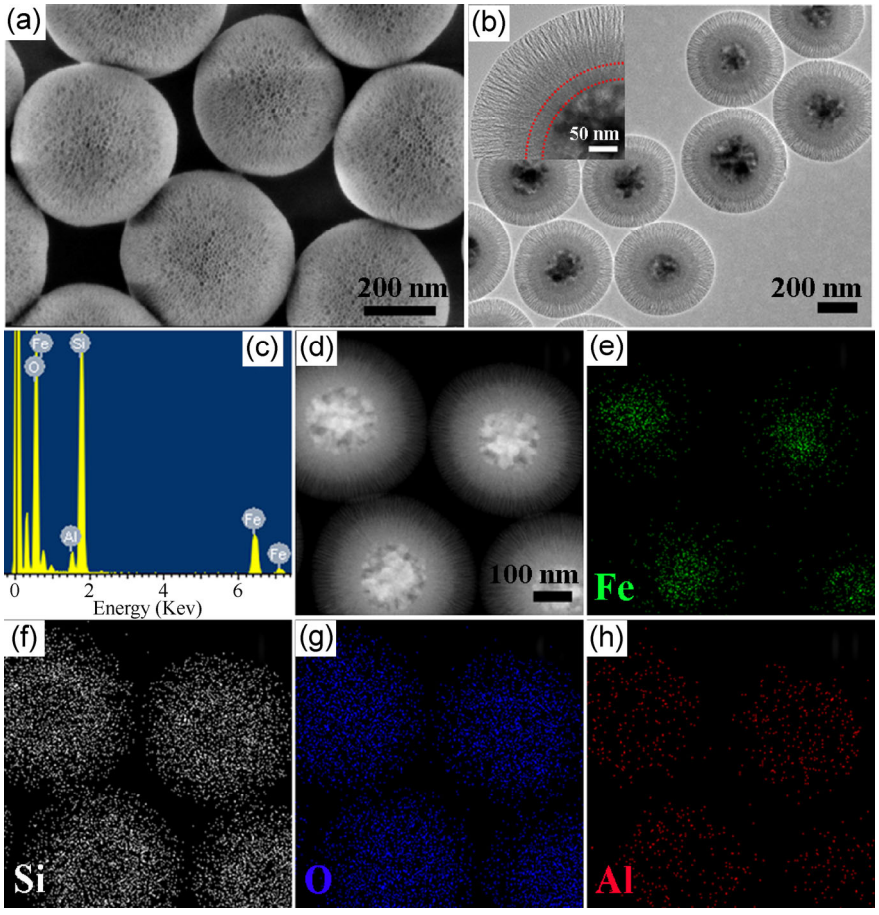

Figure 3 Monodisperse magnetic mesoporous aluminosilicate core-shell structured nanospheres with large dendritic, radially oriented mesopores and ordered mesostructures, prepared by combining oil-water biphase stratification coating with a post-synthesis strategy. (a) FESEM image; (b) TEM image; (c) EDX spectrum; (d) STEM image; (e)–(h) EDX elemental mapping of the magnetic mesoporous aluminosilicate core-shell structured nanospheres for (e) Fe, (f) Si, (g) O, and (h) Al.

(without Fe_3O_4@SiO_2 cores, Fig. S5 in the ESM) show two signals at 0 and 53 ppm, corresponding to six- and four-coordinated Al species, respectively (Fig. 4(b) and Scheme 1(e)). The NH_3-TPD experiments display a broad peak at 301 ℃, which is attributed to strong acidic sites (Fig. S6 in the ESM).

Phosphate is one of the major nutrients in water bodies and causes the eutrophication, which results in serious environmental problems. Methods for the removal of excessive phosphate include chemical precipitations with Fe, Ca, and Al components, biological treatments such as conventional activated-sludge process, and promising adsorption approaches [50, 51]. Although a variety of adsorbents are proposed for the adsorption of phosphate, the performance and kinds are still far from being satisfactory. In this work, the synthetic magnetic mesoporous aluminosilicate core-shell structured nanospheres can be rationally adopted as an ideal adsorbent for phosphate capture in wastewater. Adsorption isotherms show that Fe_3O_4@SiO_2@dendritic-mSiO_2 without Al in mesoporous frameworks presents a low phosphate adsorption capacity of ~3 mg·g^{-1} (Fig. 4(c)). Upon incorporation of Al, the nanospheres possess an impressive saturation capacity of 12.7 mg·g^{-1} for phosphates after magnetic separation (Table S1 in the ESM). The phosphate removal capacity is considerably higher than that of the conventional red mud (1.8 mg·g^{-1}) and magnetite nanoparticles (5.2 mg·g^{-1}) [51]. Markedly, the adsorption isotherm can be well satisfied by the Langmuir model, suggesting a monolayer adsorption behavior and a strong affinity for adsorption (Fig. 4(c)). Notably, the magnetic mesoporous aluminosilicate nanospheres can rapidly capture 90 wt.% of the phosphates (50 mg·L^{-1})

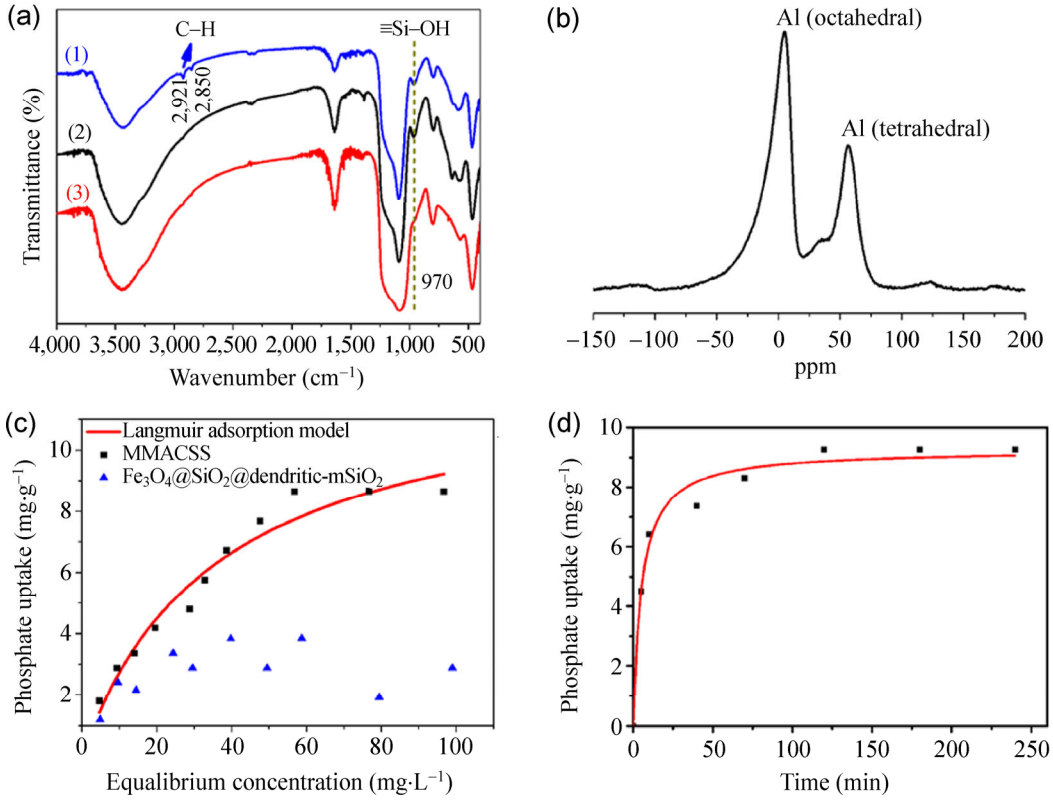

Figure 4 (a) FTIR spectra of (1) Fe_3O_4@SiO_2@dendritic-$mSiO_2$/CTAC as-prepared core-shell nanospheres, (2) Fe_3O_4@SiO_2@dendritic-$mSiO_2$ core-shell nanospheres after removal of the CTAC surfactant, and (3) monodisperse magnetic mesoporous aluminosilicate core-shell structured nanospheres. (b) ^{27}Al solid-state NMR spectrum of mesoporous aluminosilicate nanospheres (without Fe_3O_4@SiO_2 cores). (c) Adsorption isotherms at room temperature of phosphates on Fe_3O_4@SiO_2@dendritic-$mSiO_2$ and magnetic mesoporous aluminosilicate core-shell structured nanospheres. (d) Adsorption kinetics of the magnetic mesoporous aluminosilicate core-shell structured nanospheres with phosphate concentration of (50 mg·L^{-1}) and sorbent loading of (0.4 mg·mL^{-1}).

within 50 min, even with a low sorbent concentration (0.4 mg·mL^{-1}), as revealed by the adsorption kinetics (Fig. 4(d)). The adsorption kinetics provides a close fit to the pseudo second-order model with a rapid initial adsorption rate of ~0.021 g·mg^{-1}·min^{-1} (Table S2 in the ESM). The remarkable removal capacity and adsorption kinetics originate directly from the unique large dendritic open mesopore channels and Al-incorporated frameworks with considerably strong acidic sites.

4 Conclusions

In summary, we have demonstrated an effective oil-water biphase stratification coating strategy to fabricate dendritic mesoporous silica encapsulated magnetic nanospheres. The monodispersed Fe_3O_4@SiO_2@dendritic-$mSiO_2$ nanospheres have radially oriented, large open mesochannels, and controllable pore size (5.7–10.3 nm) and shell thickness (40–100 nm). With a simple impregnation, Al species can be well incorporated into the shell frameworks to obtain a dendritic mesoporous aluminosilicate core-shell structure. These elegant MMACSS nanospheres exhibit large dendritic mesopores (2.7 and 10.3 nm), and useful strong acidic sites. They also have superior magnetic properties (13.5 emu·g^{-1}) and an impressive capacity to capture phosphates (12.7 mg·g^{-1}). Moreover, we believe that this proposed strategy presents a promising platform toward the fabrication of hierarchical nanostructures with high-performance and multifunctional cores, and large dendritic mesoporous silica and aluminosilicate shell structures, thus providing more opportunities for applications in advanced catalysis and bio-related fields.

Acknowledgements

We acknowledge the financial support from State Key Laboratory of Pollution Control and Resource Reuse Foundation (No. PCRRF14017), the National Natural Science Foundation of China (No. 21210004) and the China Postdoctoral Science Foundation (No. 2014M551455). J. P. Y. appreciates the funding supported by the Commonwealth of Australia through the Automotive Australia 2020 Cooperative Research Centre (Auto CRC) and DP120101194. The authors would like to thank Dr. T. Silver for critical reading of this manuscript.

Electronic Supplementary Material: Supplementary material (SEM, TEM, XRD and NH_3-TPD) is available in the online version of this article at http://dx.doi.org/10.1007/s12274-015-0758-2.

References

[1] Lauhon, L. J.; Gudiksen, M. S.; Wang, D. L.; Lieber, C. M. Epitaxial core-shell and core-multishell nanowire heterostructures. *Nature* **2002**, *420*, 57–61.

[2] Wang, D. L.; Xin, H. L.; Hovden, R.; Wang, H. S.; Yu, Y. C.; Muller, D. A.; DiSalvo, F. J.; Abruña, H. D. Structurally ordered intermetallic platinum-cobalt core-shell nanoparticles with enhanced activity and stability as oxygen reduction electrocatalysts. *Nat. Mater.* **2013**, *12*, 81–87.

[3] Alayoglu, S.; Nilekar, A. U.; Mavrikakis, M.; Eichhorn, B. Ru-Pt core-shell nanoparticles for preferential oxidation of carbon monoxide in hydrogen. *Nat. Mater.* **2008**, *7*, 333–338.

[4] Chen, O.; Zhao, J.; Chauhan, V. P.; Cui, J.; Wong, C.; Harris, D. K.; Wei, H.; Han, H. S.; Fukumura, D.; Jain, R. K. et al. Compact high-quality CdSe-CdS core-shell nanocrystals with narrow emission linewidths and suppressed blinking. *Nat. Mater.* **2013**, *12*, 445–451.

[5] Chen, O.; Riedemann, L.; Etoc, F.; Herrmann, H.; Coppey, M.; Barch, M.; Farrar, C. T.; Zhao, J.; Bruns, O. T.; Wei, H. et al. Magneto-fluorescent core-shell supernanoparticles. *Nat. Commun.* **2014**, *5*, 5093.

[6] Bigall, N. C.; Parak, W. J.; Dorfs, D. Fluorescent, magnetic and plasmonic-hybrid multifunctional colloidal nano objects. *Nano Today* **2012**, *7*, 282–296.

[7] Chen, G. Y.; Agren, H.; Ohulchanskyy, T. Y.; Prasad, P. N. Light upconverting core-shell nanostructures: Nanophotonic control for emerging applications. *Chem. Soc. Rev.* **2015**, *44*, 1680–1713.

[8] Zhang, Q.; Lee, I.; Joo, J. B.; Zaera, F.; Yin, Y. D. Core-shell nanostructured catalysts. *Acc. Chem. Res.* **2013**, *46*, 1816–1824.

[9] Li, W.; Zhao, D. Y. Extension of the stöber method to construct mesoporous SiO_2 and TiO_2 shells for uniform multifunctional core-shell structures. *Adv. Mater.* **2013**, *25*, 142–149.

[10] Xia, Y. N.; Li, W. Y.; Cobley, C. M.; Chen, J. Y.; Xia, X. H.; Zhang, Q.; Yang, M. X.; Cho, E. C.; Brown, P. K. Gold nanocages: From synthesis to theranostic applications. *Acc. Chem. Res.* **2011**, *44*, 914–924.

[11] Reiss, P.; Protière, M.; Li, L. Core/shell semiconductor nanocrystals. *Small* **2009**, *5*, 154–168.

[12] He, L. C.; Liu, Y.; Liu, J. Z.; Xiong, Y. S.; Zheng, J. Z.; Liu, Y. L.; Tang, Z. Y. Core-shell noble-metal@metal-organic-framework nanoparticles with highly selective sensing property. *Angew. Chem. Int. Ed.* **2013**, *52*, 3741–3745.

[13] Hu, M.; Furukawa, S.; Ohtani, R.; Sukegawa, H.; Nemoto, Y.; Reboul, J.; Kitagawa, S.; Yamauchi, Y. Synthesis of prussian blue nanoparticles with a hollow interior by controlled chemical etching. *Angew. Chem. Int. Ed.* **2012**, *51*, 984–988.

[14] Li, G. L.; Mohwald, H.; Shchukin, D. G. Precipitation polymerization for fabrication of complex core-shell hybrid particles and hollow structures. *Chem. Soc. Rev.* **2013**, *42*, 3628–3646.

[15] Caruso, F.; Susha, A. S.; Giersig, M.; Möhwald, H. Magnetic core-shell particles: Preparation of magnetite multilayers on polymer latex microspheres. *Adv. Mater.* **1999**, *11*, 950–953.

[16] Li, G. L.; Xu, L. Q.; Neoh, K. G.; Kang, E. T. Hairy hybrid microrattles of metal nanocore with functional polymer shell and brushes. *Macromolecules* **2011**, *44*, 2365–2370.

[17] Li, G. L.; Tai, C. A.; Neoh, K. G.; Kang, E. T.; Yang, X. L. Hybrid nanorattles of metal core and stimuli-responsive polymer shell for confined catalytic reactions. *Polym. Chem.* **2011**, *2*, 1368–1374.

[18] Sun, X. M.; Li, Y. D. Colloidal carbon spheres and their core/shell structures with noble-metal nanoparticles. *Angew. Chem. Int. Ed.* **2004**, *43*, 597–601.

[19] Park, J. C.; Song, H. Metal@silica yolk-shell nanostructures as versatile bifunctional nanocatalysts. *Nano Res.* **2011**, *4*, 33–49.

[20] Guerrero-Martínez, A.; Pérez-Juste, J.; Liz-Marzán, L. M. Recent progress on silica coating of nanoparticles and related nanomaterials. *Adv. Mater.* **2010**, *22*, 1182–1195.

[21] Zhong, C. J.; Maye, M. M. Core–shell assembled nanoparticles as catalysts. *Adv. Mater.* **2001**, *13*, 1507–1511.

[22] Lou, X. W.; Archer, L. A.; Yang, Z. C. Hollow micro-/nanostructures: Synthesis and applications. *Adv. Mater.* **2008**, *20*, 3987–4019.

[23] Liz-Marzán, L. M.; Mulvaney, P. The assembly of coated nanocrystals. *J. Phy. Chem. B* **2003**, *107*, 7312–7326.

[24] Li, Z. J.; Zhao, J.; Zhang, M.; Xia, J. Y.; Meng, A. SiC nanowires with thickness-controlled SiO_2 shells: Fabrication, mechanism, reaction kinetics and photoluminescence properties. *Nano Res.* **2014**, *7*, 462–472.

[25] Chen, J. C.; Zhang, R. Y.; Han, L.; Tu, B.; Zhao, D. Y. One-pot synthesis of thermally stable gold@mesoporous silica core-shell nanospheres with catalytic activity. *Nano Res.* **2013**, *6*, 871–879.

[26] Zhang, M. L.; Earhart, C.; Ooi, C.; Wilson, R.; Tang, M.; Wang, S. Functionalization of high-moment magnetic nano-disks for cell manipulation and separation. *Nano Res.* **2013**, *6*, 745–751.

[27] Wang, Y.; Gu, H. C. Core-shell-type magnetic mesoporous silica nanocomposites for bioimaging and therapeutic agent delivery. *Adv. Mater.* **2015**, *27*, 576–585.

[28] Joo, S. H.; Park, J. Y.; Tsung, C. K.; Yamada, Y.; Yang, P. D.; Somorjai, G. A. Thermally stable Pt/mesoporous silica core-shell nanocatalysts for high-temperature reactions. *Nat. Mater.* **2009**, *8*, 126–131.

[29] Liu, J.; Qiao, S. Z.; Hartono, S. B.; Lu, G. Q. Monodisperse yolk-shell nanoparticles with a hierarchical porous structure for delivery vehicles and nanoreactors. *Angew. Chem. Int. Ed.* **2010**, *49*, 4981–4985.

[30] Pérez-Lorenzo, M.; Vaz, B.; Salgueiriño, V.; Correa-Duarte, M. A. Hollow-shelled nanoreactors endowed with high catalytic activity. *Chem.—Eur. J.* **2013**, *19*, 12196–12211.

[31] Xu, Z. C.; Hou, Y. L.; Sun, S. H. Magnetic core/shell Fe_3O_4/Au and Fe_3O_4/Au/Ag nanoparticles with tunable plasmonic properties. *J. Am. Chem. Soc.* **2007**, *129*, 8698–8699.

[32] Wong, Y. J.; Zhu, L. F.; Teo, W. S.; Tan, Y. W.; Yang, Y. H.; Wang, C.; Chen, H. Y. Revisiting the stöber method: Inhomogeneity in silica shells. *J. Am. Chem. Soc.* **2011**, *133*, 11422–11425.

[33] Ge, J. P.; Zhang, Q.; Zhang, T. R.; Yin, Y. D. Core-satellite nanocomposite catalysts protected by a porous silica shell: Controllable reactivity, high stability, and magnetic recyclability. *Angew. Chem. Int. Ed.* **2008**, *47*, 8924–8928.

[34] Zhao, W. R.; Gu, J. L.; Zhang, L. X.; Chen, H. R.; Shi, J. L. Fabrication of uniform magnetic nanocomposite spheres with a magnetic core/mesoporous silica shell structure. *J. Am. Chem. Soc.* **2005**, *127*, 8916–8917.

[35] Kim, J.; Kim, H. S.; Lee, N.; Kim, T.; Kim, H.; Yu, T.; Song, I. C.; Moon, W. K.; Hyeon, T. Multifunctional uniform nanoparticles composed of a magnetite nanocrystal core and a mesoporous silica shell for magnetic resonance and fluorescence imaging and for drug delivery. *Angew. Chem. Int. Ed.* **2008**, *47*, 8438–8441.

[36] Deng, Y. H.; Qi, D. W.; Deng, C. H.; Zhang, X. M.; Zhao, D. Y. Superparamagnetic high-magnetization microspheres with an Fe_3O_4@SiO_2 core and perpendicularly aligned mesoporous SiO_2 shell for removal of microcystins. *J. Am. Chem. Soc.* **2008**, *130*, 28–29.

[37] Yang, J. P.; Shen, D. K.; Zhou, L.; Li, W.; Fan, J. W.; El-Toni, A. M.; Zhang, W. X.; Zhang, F.; Zhao, D. Y. Mesoporous silica-coated plasmonic nanostructures for surface-enhanced Raman scattering detection and photothermal therapy. *Adv. Healthcare Mater.* **2014**, *3*, 1620–1628.

[38] Yang, J. P.; Shen, D. K.; Zhou, L.; Li, W.; Li, X. M.; Yao, C.; Wang, R.; El-Toni, A. M.; Zhang, F.; Zhao, D. Y. Spatially confined fabrication of core-shell gold nanocages@mesoporous silica for near-infrared controlled photothermal drug release. *Chem. Mater.* **2013**, *25*, 3030–3037.

[39] Yang, J. P.; Zhang, F.; Chen, Y. R.; Qian, S.; Hu, P.; Li, W.; Deng, Y. H.; Fang, Y.; Han, L.; Luqman, M. et al. Core-shell Ag@SiO_2@mSiO_2 mesoporous nanocarriers for metal-enhanced fluorescence. *Chem. Commun.* **2011**, *47*, 11618–11620.

[40] Yang, J. P.; Zhang, F.; Li, W.; Gu, D.; Shen, D. K.; Fan, J. W.; Zhang, W. X.; Zhao, D. Y. Large pore mesostructured cellular silica foam coated magnetic oxide composites with multilamellar vesicle shells for adsorption. *Chem. Commun.* **2014**, *50*, 713–715.

[41] Qian, X. F.; Du, J. M.; Li, B.; Si, M.; Yang, Y. S.; Hu, Y. Y.; Niu, G. X.; Zhang, Y. H.; Xu, H. L.; Tu, B. et al. Controllable fabrication of uniform core-shell structured zeolite@SBA-15 composites. *Chem. Sci.* **2011**, *2*, 2006–2016.

[42] Yang, J. P.; Qian, X. F.; Chen, M. J.; Fan, J. W.; Liu, H. K.; Zhang, W. X. A triblock-copolymer-templating route to carbon spheres@SBA-15 large mesopore core-shell and hollow structures. *RSC Adv.* **2014**, *4*, 48676–48681.

[43] Fang, X. L.; Liu, Z. H.; Hsieh, M. F.; Chen, M.; Liu, P. X.; Chen, C.; Zheng, N. F. Hollow mesoporous aluminosilica spheres with perpendicular pore channels as catalytic nanoreactors. *ACS Nano* **2012**, *6*, 4434–4444.

[44] Du, X.; Qiao, S. Z. Dendritic silica particles with center-radial pore channels: Promising platforms for catalysis and biomedical applications. *Small* **2015**, *11*, 392–413.

[45] Shen, D. K.; Yang, J. P.; Li, X. M.; Zhou, L.; Zhang, R. Y.; Li, W.; Chen, L.; Wang, R.; Zhang, F.; Zhao, D. Y. Biphase stratification approach to three-dimensional dendritic biodegradable mesoporous silica nanospheres. *Nano Lett.* **2014**, *14*, 923–932.

[46] Du, X.; Shi, B. Y.; Liang, J.; Bi, J. X.; Dai, S.; Qiao, S. Z. Developing functionalized dendrimer-like silica nanoparticles with hierarchical pores as advanced delivery nanocarriers. *Adv. Mater.* **2013**, *25*, 5981–5985.

[47] Polshettiwar, V.; Cha, D.; Zhang, X. X.; Basset, J. M. High-surface-area silica nanospheres (KCC-1) with a fibrous morphology. *Angew. Chem. Int. Ed.* **2010**, *49*, 9652–9656.

[48] Yang, J. P.; Chen, W. Y.; Shen, D. K.; Wei, Y.; Ran, X. Q.; Teng, W.; Fan, J. W.; Zhang, W. X.; Zhao, D. Y. Controllable fabrication of dendritic mesoporous silica-carbon nanospheres for anthracene removal. *J. Mater. Chem. A* **2014**, *2*, 11045–11048.

[49] Yang, Y. N.; Niu, Y. T.; Zhang, J.; Meka, A. K.; Zhang, H. W.; Xu, C.; Lin, C. X. C.; Yu, M. H.; Yu, C. Z. Biphasic synthesis of large-pore and well-dispersed benzene bridged mesoporous organosilica nanoparticles for intracellular protein delivery. *Small*, in press, DOI: 10.1002/smll.201402779.

[50] Shin, E. W.; Han, J. S.; Jang, M.; Min, S. H.; Park, J. K.; Rowell, R. M. Phosphate adsorption on aluminum-impregnated mesoporous silicates: Surface structure and behavior of adsorbents. *Environ. Sci. Technol.* **2004**, *38*, 912–917.

[51] Yang, J.; Zhou, L.; Zhao, L. Z.; Zhang, H. W.; Yin, J. N.; Wei, G. F.; Qian, K.; Wang, Y. H.; Yu, C. Z. A designed nanoporous material for phosphate removal with high efficiency. *J. Mater. Chem.* **2011**, *21*, 2489–2494.